LAWRENCE
LIVERMORE
NATIONAL
LABORATORY

LLNL-PROC-410959

A Comparison of Monte Carlo Particle Transport Algorithms for Binary Stochastic Mixtures

P. S. Brantley

March 2, 2009

2009 International Conference on Advances in Mathematics, Computational Methods, and Reactor Physics
Saratoga Springs, NY, United States
May 3, 2009 through May 7, 2009

Disclaimer

International Conference on Mathematics, Computational Methods & Reactor Physics (M&C 2009)
Saratoga Springs, New York, May 3-7, 2009, on CD-ROM, American Nuclear Society, LaGrange Park, IL (2009)

A COMPARISON OF MONTE CARLO PARTICLE TRANSPORT ALGORITHMS FOR BINARY STOCHASTIC MIXTURES

Patrick S. Brantley
Lawrence Livermore National Laboratory
P.O. Box 808, L-023
Livermore, CA 94551 USA
brantley1@llnl.gov

ABSTRACT

Two Monte Carlo algorithms originally proposed by Zimmerman and Zimmerman and Adams for particle transport through a binary stochastic mixture are numerically compared using a standard set of planar geometry benchmark problems. In addition to previously-published comparisons of the ensemble-averaged probabilities of reflection and transmission, we include comparisons of detailed ensemble-averaged total and material scalar flux distributions. Because not all benchmark scalar flux distribution data used to produce plots in previous publications remains available, we have independently regenerated the benchmark solutions including scalar flux distributions. Both Monte Carlo transport algorithms robustly produce physically-realistic scalar flux distributions for the transport problems examined. The first algorithm reproduces the standard Levermore-Pomraning model results for the probabilities of reflection and transmission. The second algorithm generally produces significantly more accurate probabilities of reflection and transmission and also significantly more accurate total and material scalar flux distributions.

Key Words: Monte Carlo particle transport, binary stochastic mixture

1. INTRODUCTION

Particle transport through binary stochastic mixtures has received considerable research attention in the last two decades [1, 2]. Much of the research has focused on the development and analysis of approximate deterministic models for the solution of such particle transport problems. The most ubiquitous approximate deterministic model is often referred to as the Levermore-Pomraning or the Standard Model [2]. A comparatively limited amount of research has been performed into the development of Monte Carlo algorithms for the solution of these problems. Zimmerman [3] and Zimmerman and Adams [4] proposed a Monte Carlo algorithm that solves the Levermore-Pomraning equations (Algorithm A) and another Monte Carlo algorithm that should possess improved accuracy (Algorithm B). Donovan and Danon [5] applied the Levermore-Pomraning algorithm proposed by Zimmerman (Algorithm A) to the specific case of a two-dimensional binary stochastic mixture composed of circular disks of one material randomly distributed in a background matrix material. Donovan and Danon generally refer to these types of Monte Carlo algorithms as "chord length sampling" (CLS) algorithms. Donovan and Danon also examined a "limited chord length sampling" (LCLS) algorithm for their problem in which the particle transport through the disks is modelled explicitly, and the transport through the background material is treated using CLS (Algorithm A). Donovan and Danon did not examine for their specific problem the approach of using Algorithm B for both materials in the problem. We focus in this paper on the algorithms proposed by Zimmerman and Zimmerman and Adams applied consistently over the one-dimensional spatial domain.

Zimmerman and Adams [4] numerically demonstrated that the base algorithm (Algorithm A) solves the Levermore-Pomraning equations and that the improved algorithm (Algorithm B) is more accurate by comparing the results of these algorithms to a standard set of planar geometry binary stochastic mixture benchmark transport solutions [6]. The benchmark transport problems involve an isotropic angular flux incident on one boundary of a binary Markovian statistical planar geometry medium, and the benchmark quantities tabulated are reflection and transmission probabilities. Zuchuat et al. [7] reproduced the Markovian statistics benchmark results published in Ref. [6] and extended these benchmark solutions to additional non-Markovian material statistics. In addition to the probabilities of reflection and transmission, Zuchuat et al. tabulated the ensemble-averaged total and material scalar flux distributions. In this paper, we extend for the first time the comparisons of the Monte Carlo algorithms proposed by Zimmerman [3] and Zimmerman and Adams [4] to include the scalar flux distributions produced. This comparison is important, because as demonstrated in Ref. [7], an approximate model that gives accurate reflection and transmission probabilities can produce unphysical scalar flux distributions. Our numerical results demonstrate that for the benchmark transport problems considered, Algorithms A and B robustly produce physically-realistic scalar flux distributions. This result for Algorithm A is largely expected (although not previously demonstrated), because that algorithm solves the Levermore-Pomraning equations; the demonstration of this fact for Algorithm B is new. The scalar flux distributions produced by Algorithm B are generally more accurate than those produced by Algorithm A.

The remainder of this paper is organized as follows. In Section 2, we describe the benchmark transport problem that we use to assess the accuracy of the Monte Carlo algorithms. In Section 3, we outline the Monte Carlo algorithms proposed by Zimmerman and Zimmerman and Adams for the solution of particle transport through stochastic media. We then present the numerical comparisons of the algorithms in Section 4. We give general conclusions and suggestions for future work in Section 5.

2. BENCHMARK TRANSPORT PROBLEMS

We consider the following time-independent monoenergetic neutron transport problem [6] with isotropic scattering in a one-dimensional planar geometry spatial domain defined on $0 \leq x \leq L$:

$$\mu \frac{\partial}{\partial x} \psi(x,\mu) + \sigma_t(x)\,\psi(x,\mu) = \frac{1}{2}\sigma_s(x) \int_{-1}^{1} \psi(x,\mu')\,d\mu' \ , \ 0 \leq x \leq L \ , -1 \leq \mu \leq 1 \ , \quad (1)$$

$$\psi(0,\mu) = 2 \ , \ \mu > 0 \ , \quad (2)$$

$$\psi(L,\mu) = 0 \ , \ \mu < 0 \ . \quad (3)$$

Eqs. (1)–(3) are written in standard neutronics notation [8]. The boundary conditions given by Eqs. (2) and (3) are nonstochastic and represent an isotropic incident angular flux with a unity partial incoming current at $x = 0$ and a vacuum boundary at $x = L$. The stochastic spatial medium is assumed to be composed of alternating slabs of two materials, labelled with the indices 0 and 1, with the mean material slab width for material i denoted as Λ_i. The total and scattering cross sections for each material are uniform and are denoted as σ_t^i and σ_s^i, $i = 0, 1$, respectively. The distribution of material slab widths in the planar medium is assumed to be described by

spatially homogeneous Markovian statistics [2], in which case a slab width for material i, λ_i, can be sampled from an exponential distribution given by

$$f_i(\lambda_i) = \frac{1}{\Lambda_i} \exp\left(-\frac{\lambda_i}{\Lambda_i}\right) \quad , \tag{4}$$

where again Λ_i is the mean material slab width for material i. Given the mean material slab widths, the probability of finding material i at any given point in the spatial domain, p_i, is given by

$$p_i = \frac{\Lambda_i}{\Lambda_0 + \Lambda_1} \quad . \tag{5}$$

This material probability corresponds to the volume fraction of the material in the problem.

The typical fiducial comparison quantities of interest are the ensemble-averaged probability of reflection from the slab, $\langle R \rangle$, defined as

$$\langle R \rangle = \int_{-1}^{0} |\mu| \langle \psi(0,\mu) \rangle \, d\mu \quad , \tag{6}$$

and the ensemble-averaged probability of transmission through the slab, $\langle T \rangle$, defined as

$$\langle T \rangle = \int_{0}^{1} \mu \langle \psi(L,\mu) \rangle \, d\mu \quad . \tag{7}$$

In addition, we are interested in comparing the ensemble-averaged total and material scalar flux distributions, $\langle \phi(x) \rangle$ and $\langle \phi_i(x) \rangle$, $i = 0, 1$, respectively, as these distributions determine reaction rates in the system.

The material parameters for the benchmark transport problems are given in Table I using the notation of Ref. [7]. The scattering ratio for material i is defined as $c_i = \sigma_s^i / \sigma_t^i$. For each set of material parameters (cases 1, 2, and 3), three sets of scattering ratio combinations (cases a, b, and c) and three slab widths (L = 0.1, 1.0, and 10.0) are considered. For all cases, the ensemble-averaged total cross section, defined as $\langle \sigma_t \rangle = p_0 \sigma_t^0 + p_1 \sigma_t^1$, is unity. The different case numbers (i.e. 1, 2, and 3) represent permutations of materials with mean materal slab widths of optical depth 0.1, 1.0, and 10.0. The different case letters (i.e. a, b, and c) represent varying amounts of scattering for each material.

Table I. Material parameters for benchmark transport problems

Case	σ_t^0	Λ_0	σ_t^1	Λ_1	Case	c_0	c_1	L
1	10/99	99/100	100/11	11/100	a	0.0	1.0	0.1
2	10/99	99/10	100/11	11/10	b	1.0	0.0	1.0
3	2/101	101/20	200/101	101/20	c	0.9	0.9	10.0

Because not all of the benchmark scalar flux distribution data previously published [7] in graphical form remains available [9], we have independently regenerated the benchmark solutions

including scalar flux distributions using the methodologies described in Refs. [6] and [7]. These benchmark solutions were computed with a discrete ordinates transport code using a standard S_{16} Gauss-Legendre quadrature set and the linear discontinuous spatial discretization with a mesh spacing in each material such that $\frac{\sigma_t^i \Delta x}{|\mu|_{min}} \leq \frac{1}{10}$, where $|\mu|_{min}$ is the minimum cosine in the quadrature set [8]. 10^5 independent statistical material realizations (the same number as in Refs. [6] and [7]) were sampled from Markovian statistics and simulated for each case. The ensemble-averaged total and material scalar flux distributions were tallied at the edges of 100 uniformly-spaced spatial zones. (We enforced a minimum of 100 spatial zones for each independent material realization.) We have verified these benchmark solutions against the probabilities of reflection and transmission published in Refs. [6] and [7], finding agreement to typically two to three digits, and against the scalar flux distribution data remaining available [9] from Ref. [7].

3. MONTE CARLO ALGORITHMS

In this section, we describe in more detail the Monte Carlo Algorithms A and B proposed by Zimmerman [3] and Zimmerman and Adams [4] for solving the benchmark transport problem described above. For both Algorithms A and B, a particle history begins with sampling the source particle characteristics by setting the spatial position $x = 0$, sampling a direction of flight cosine μ from a cosine distribution representing the isotropic incident angular flux, and sampling a material identifier for the particle according to the probabilities defined in Eq. (5). Next, distances to the required events are either sampled or computed. The distance to collision, d_c, is sampled using the macroscopic total cross section corresponding to the material in which the particle exists. Because we are interested in comparing the total and material scalar flux distributions, we impose a uniform spatial mesh on the spatial domain in which to tally this information. As a result, we introduce a new distance calculation, the distance to zone boundary, d_b, computed using the current position and direction of flight of the particle and the boundaries of the spatial zone in which the particle exists. We compute the Monte Carlo scalar flux tallies using a track length estimator [8]. The tally volume for the total scalar flux is the zone volume. The tally volume for a material scalar flux is the zone volume times the volume fraction of the material in the zone, where the volume fraction of material i is equal to the material probability p_i defined in Eq. (5). For both Monte Carlo algorithms, the distance the particle travels in the zone is tallied whenever a particle is moved.

In the next sections, we describe in more detail the particle history flow for Algorithms A and B.

3.1. Algorithm A: The Levermore-Pomraning Solution

For each particle history:

1. Compute d_b and sample d_c as described above.
2. Sample the distance to material interface, d_i, by first sampling a material slab width from the exponential distribution given by Eq. (4) and then dividing by the particle angle to account for the direction of particle motion, i.e. $d_i = -\lambda_i \ln(\xi)/|\mu|$, where ξ is a random number.

3. Compute the minimum of d_b, d_c, and d_i to determine the event.
4. If d_b is the minimum distance, move the particle to the zone boundary. If the particle is escaping the spatial domain, update the appropriate reflection or transmission tally, terminate the history, and track the next particle. Otherwise, return to step 1.
5. If d_c is the minimum distance, move the particle the appropriate distance, and sample the collision type using the macroscopic total and scattering cross sections for the material in which the particle exists. If the sampled collision is absorption, terminate the history and track the next particle. If the sampled collision is scattering, perform the scattering collision by sampling the outgoing characteristics of the scattered particle; the particle maintains its current material identifier. Return to step 1.
6. If d_i is the minimum distance, move the particle the appropriate distance and switch the material identifier. Return to step 1.

Note that following a collision, a new distance to material interface is sampled. As a result, the particle encounters a different material realization following a collision, which is unphysical. As noted by Zimmerman and Adams [4], this algorithm is exact in a purely absorbing medium. We expect Algorithm A to be less accurate in highly scattering materials with optically thick mean material slab widths. Because we have imposed a spatial mesh on the problem, a new distance to material interface is also sampled following a zone boundary crossing.

3.2. Algorithm B: A More Accurate Solution

For each particle history:

1. Sample the distance to material interface in the forward direction of particle motion, d_i^+, as described in Algorithm A. Set the the distance to material interface in the backward direction, d_i^-, to zero.
2. Compute d_b and sample d_c as described above.
3. Compute the minimum of d_b, d_c, and d_i^+ to determine the event.
4. If d_b is the minimum distance, initially treat as in Algorithm A. In addition, adjust the distance to material interface values in the forward and backward directions to account for the distance the particle was moved. Return to step 2.
5. If d_c is the minimum distance, initially treat as in Algorithm A. In addition, adjust the distance to material interface values in the forward and backward directions to account for the distance the particle was moved. If the sampled collision is scattering, also adjust the distance to material interface values in the forward and backward directions to account for the change in direction of flight of the particle after the scatter. Switch the forward and backward distance to material interface values if the particle is backscattered (i.e. the value of μ changes sign). Return to step 2.
6. If d_i^+ is the minimum distance, move the particle the appropriate distance, switch the material identifier, sample a new d_i^+, and set d_i^- to zero. Return to step 2.

In Algorithm B, a particle can move within one material and encounter the same realization, which is more physically realistic than Algorithm A. As a result, we expect Algorithm B to be more accurate than Algorithm A.

4. NUMERICAL COMPARISONS TO BENCHMARK PROBLEMS

In this section, we evaluate the accuracy of the Monte Carlo algorithms described in Section 3 using the set of benchmark problems described in Section 2. In addition to comparisons of the probabilities of transmission and reflection previously published by Zimmerman and Adams [4], we compare for the first time the detailed scalar flux distributions produced by these Monte Carlo algorithms with the benchmark scalar flux distributions. The scalar flux distributions were tallied in the Monte Carlo simulations using 100 uniform spatial zones. Each Monte Carlo simulation was performed using 10^7 particle histories, resulting in pointwise relative standard deviations for the material scalar flux distributions of typically much less than 1%.

We compare the accuracy of the ensemble-averaged probabilities of reflection and transmission computed using the Monte Carlo algorithms to the benchmark values using relative errors computed as

$$E_{\langle X\rangle} = \frac{\langle X\rangle_{MC} - \langle X\rangle_{benchmark}}{\langle X\rangle_{benchmark}} \ , \tag{8}$$

where $\langle X\rangle$ represents either the ensemble-averaged probability of reflection, $\langle R\rangle$, or transmission, $\langle T\rangle$. We compare the accuracy of the scalar flux distributions using a root-mean-squared (RMS) relative error computed as

$$E_{\langle\phi\rangle} = \sqrt{\frac{1}{N}\sum_{j=0}^{N-1}\left(\frac{\left\langle\phi^j_{MC}\right\rangle - \left\langle\phi^j_{benchmark}\right\rangle}{\left\langle\phi^j_{benchmark}\right\rangle}\right)^2} \ , \tag{9}$$

where $\langle\phi\rangle$ represents the ensemble-averaged total or material scalar flux distribution, $\langle\phi\left(x\right)\rangle$ or $\langle\phi_i\left(x\right)\rangle$, $i = 0, 1$, respectively, and the summation is over the $N = 100$ spatial tally zones. The Monte Carlo scalar flux tallies were computed using track length estimators in the spatial zones. The benchmark scalar flux results were computed using a discrete ordinates code with a linear discontinuous spatial discretization [8]. We compare the Monte Carlo zonal scalar flux tally with the discrete ordinates cell-average value computed as the algebraic average of the cell-edge values (consistent with the linear discontinous discretization).

The computed Monte Carlo results for the reflection and transmission probabilities for cases 1 through 3 are shown in Tables II–IV. The RMS relative error results for the total and material scalar flux distributions for cases 1 through 3 are shown in Tables V–VII. The total and material scalar flux distributions computed by the benchmark procedure and the Monte Carlo algorithms for all cases with $L = 10$ are plotted in Figs. 1–9.

The Algorithm A reflection and transmission probability results agree in all cases, to typically two to three digits, with previously-published Levermore-Pomraning model results [6, 7]. (We have not verified in detail that the scalar flux distributions produced by Algorithm A agree with the distributions produced by deterministic solutions of the Levermore-Pomraning model, although we expect that they do). The Algorithm B reflection and transmission probability results

agree, as far as can be discerned, with the subset of data published as relative errors in graphical form in Ref. [4].

Two general trends can be observed from our numerical results. First, the accuracy of Algorithms A and B, as measured by the probabilities of reflection and transmission, generally improves as the slab width decreases. Second, both Algorithms A and B generally underpredict the reflection probability and overpredict the transmission probability. These trends are consistent with observations by previous researchers [4, 6, 7] from similar numerical results.

Focusing on the scalar flux distribution RMS relative error results in Tables V–VII, the accuracy of both Algorithms A and B generally improves as the slab width decreases. In general, when Algorithm A is reasonably accurate (i.e. within a couple of percent of the benchmark solution), Algorithm B is typically somewhat more accurate. When Algorithm A produces very inaccurate scalar flux distributions (i.e. larger than approximately 25% relative differences compared to the benchmark solution), Algorithm B is usually significantly more accurate. The overall Algorithm B RMS relative errors in the scalar flux distributions for the three cases examined are about a factor of one and one-half to six times smaller than the Algorithm A errors. Examining the total and material scalar flux distributions in Figs. 1–9, the Algorithm B scalar flux distributions are clearly in overall better agreement with the benchmark distributions than the Algorithm A distributions. The statistical fluctuations evident in some of the benchmark flux distributions derive from a small material probability resulting in a relatively small number of realizations contributing to the distribution. These statistical fluctuations were also observed in previous benchmark comparisons [7].

As described in Section 3.1, we expect Algorithm A to be least accurate in scattering materials with optically thick mean material slab widths. One particular example of this phenomenon is represented by case 2c for the $L = 10$ slab. For this case, materials zero and one have mean material slab widths of one and ten, respectively, and both materials have a scattering ratio of 0.9. The RMS relative scalar flux error values, given in Table VI, are 0.104 for material zero and 0.630 for material one. The error in the more optically-thick material one is significantly larger than in the less optically-thick material zero. Algorithm B is significantly more accurate than Algorithm A for this case, having RMS relative error values of 0.024 and 0.096 for materials zero and one, respectively.

Finally, we note that both Algorithms A and B produce physically-realistic total and material scalar flux distributions for the benchmark transport problems considered. This result is largely expected for Algorithm A, because it has been shown to produce the Levermore-Pomraning reflection and transmission probability results; the demonstration of this fact for Algorithm B is new. The ability of an algorithm to accurately compute scalar flux distributions is important, as these distributions determine the reaction rates in the materials.

Table II. Reflection and transmission probability comparisons for case 1

						Relative Error $E_{\langle R\rangle,\langle T\rangle}$	
L	Case	Quantity	Benchmark	Algorithm A	Algorithm B	Algorithm A	Algorithm B
0.1	a	$\langle R\rangle$ $\langle T\rangle$	0.04864 0.93650	0.04768 0.93463	0.04876 0.93350	-0.020 -0.002	0.002 -0.003
	b	$\langle R\rangle$ $\langle T\rangle$	0.00868 0.90432	0.00847 0.90062	0.00860 0.90080	-0.024 -0.004	-0.009 -0.004
	c	$\langle R\rangle$ $\langle T\rangle$	0.04814 0.93690	0.04711 0.93461	0.04807 0.93376	-0.021 -0.002	-0.001 -0.003
1.0	a	$\langle R\rangle$ $\langle T\rangle$	0.25084 0.59614	0.21898 0.62733	0.23932 0.60732	-0.127 0.052	-0.046 0.019
	b	$\langle R\rangle$ $\langle T\rangle$	0.05509 0.48611	0.04555 0.48439	0.05267 0.48505	-0.173 -0.004	-0.044 -0.002
	c	$\langle R\rangle$ $\langle T\rangle$	0.25604 0.60222	0.21693 0.62732	0.24059 0.61110	-0.153 0.042	-0.060 0.015
10.0	a	$\langle R\rangle$ $\langle T\rangle$	0.43596 0.01465	0.37823 0.02632	0.40110 0.02204	-0.132 0.797	-0.080 0.504
	b	$\langle R\rangle$ $\langle T\rangle$	0.08614 0.00164	0.05885 0.00155	0.07763 0.00163	-0.317 -0.055	-0.099 -0.006
	c	$\langle R\rangle$ $\langle T\rangle$	0.47999 0.01606	0.36962 0.02384	0.40695 0.02096	-0.230 0.484	-0.152 0.305
					RMS of $E_{\langle R\rangle}$	0.164	0.072
					RMS of $E_{\langle T\rangle}$	0.312	0.197

5. CONCLUSIONS

We have numerically compared two Monte Carlo algorithms originally proposed by Zimmerman and Zimmerman and Adams for particle transport through a binary stochastic mixture using a standard set of planar geometry benchmark problems. In addition to previously-published comparisons of the ensemble-averaged probabilities of reflection and transmission, we compared the detailed ensemble-averaged total and material scalar flux distributions. Because not all benchmark scalar flux distribution data used to produce the plots in previous publications remains available, we have independently regenerated the benchmark solutions including scalar flux distributions. Algorithm B generally produces significantly more accurate probabilities of reflection and transmission than Algorithm A and also significantly more accurate total and material scalar flux distributions. Both Monte Carlo transport algorithms robustly produce

Table III. Reflection and transmission probability comparisons for case 2

						Relative Error $E_{\langle R\rangle,\langle T\rangle}$	
L	Case	Quantity	Benchmark	Algorithm A	Algorithm B	Algorithm A	Algorithm B
0.1	a	$\langle R\rangle$ $\langle T\rangle$	0.04322 0.94194	0.04310 0.93917	0.04323 0.93912	-0.003 -0.003	0.000 -0.003
	b	$\langle R\rangle$ $\langle T\rangle$	0.00891 0.91725	0.00876 0.91410	0.00882 0.91404	-0.017 -0.003	-0.010 -0.003
	c	$\langle R\rangle$ $\langle T\rangle$	0.04270 0.94266	0.04239 0.93984	0.04245 0.93977	-0.007 -0.003	-0.006 -0.003
1.0	a	$\langle R\rangle$ $\langle T\rangle$	0.12035 0.72753	0.10695 0.74066	0.12045 0.72739	-0.111 0.018	0.001 -0.000
	b	$\langle R\rangle$ $\langle T\rangle$	0.07468 0.76241	0.07064 0.75920	0.07322 0.75950	-0.054 -0.004	-0.020 -0.004
	c	$\langle R\rangle$ $\langle T\rangle$	0.14342 0.77106	0.12445 0.77409	0.14182 0.76863	-0.132 0.004	-0.011 -0.003
10.0	a	$\langle R\rangle$ $\langle T\rangle$	0.23537 0.09844	0.18050 0.12833	0.22242 0.10605	-0.233 0.304	-0.055 0.077
	b	$\langle R\rangle$ $\langle T\rangle$	0.29034 0.19582	0.21851 0.17921	0.28552 0.19528	-0.247 -0.085	-0.017 -0.003
	c	$\langle R\rangle$ $\langle T\rangle$	0.43560 0.18721	0.28966 0.19482	0.40097 0.19560	-0.335 0.041	-0.079 0.045
					RMS of $E_{\langle R\rangle}$	0.170	0.034
					RMS of $E_{\langle T\rangle}$	0.106	0.030

physically-realistic scalar flux distributions for the transport problems examined. The demonstration of this fact for Algorithm B is new and is important, because an approximate model that gives accurate reflection and transmission probabilities can produce unphysical scalar flux distributions.

In future work, we plan to provide comparisons of these Monte Carlo algorithms for additional problems either of the benchmark variety as in this paper or problems for which analytic solutions are available.

Table IV. Reflection and transmission probability comparisons for case 3

						Relative Error $E_{\langle R\rangle,\langle T\rangle}$	
L	Case	Quantity	Benchmark	Algorithm A	Algorithm B	Algorithm A	Algorithm B
0.1	a	$\langle R\rangle$ $\langle T\rangle$	0.07583 0.92522	0.07488 0.92313	0.07495 0.92308	-0.013 -0.002	-0.012 -0.002
	b	$\langle R\rangle$ $\langle T\rangle$	0.00099 0.85329	0.00099 0.85192	0.00099 0.85179	0.000 -0.002	0.000 -0.002
	c	$\langle R\rangle$ $\langle T\rangle$	0.06700 0.91670	0.06618 0.91451	0.06613 0.91460	-0.012 -0.002	-0.013 -0.002
1.0	a	$\langle R\rangle$ $\langle T\rangle$	0.32166 0.66222	0.31548 0.66557	0.32027 0.66080	-0.019 0.005	-0.004 -0.002
	b	$\langle R\rangle$ $\langle T\rangle$	0.00886 0.48490	0.00839 0.48293	0.00873 0.48282	-0.053 -0.004	-0.015 -0.004
	c	$\langle R\rangle$ $\langle T\rangle$	0.24397 0.60683	0.23747 0.60883	0.24234 0.60533	-0.027 0.003	-0.007 -0.002
10.0	a	$\langle R\rangle$ $\langle T\rangle$	0.69171 0.16368	0.60769 0.24029	0.65412 0.19794	-0.121 0.468	-0.054 0.209
	b	$\langle R\rangle$ $\langle T\rangle$	0.03698 0.07729	0.02395 0.07565	0.03600 0.07656	-0.352 -0.021	-0.027 -0.009
	c	$\langle R\rangle$ $\langle T\rangle$	0.44745 0.10504	0.32584 0.11960	0.39879 0.11806	-0.272 0.139	-0.109 0.124
					RMS of $E_{\langle R\rangle}$	0.155	0.042
					RMS of $E_{\langle T\rangle}$	0.163	0.081

Table V. Scalar flux comparisons for case 1

			RMS Relative Error $E_{\langle\phi\rangle}$	
L	Case	Quantity	Algorithm A	Algorithm B
0.1	a	$\langle\phi\rangle$	0.010	0.010
		$\langle\phi_0\rangle$	0.010	0.011
		$\langle\phi_1\rangle$	0.007	0.004
	b	$\langle\phi\rangle$	0.004	0.004
		$\langle\phi_0\rangle$	0.004	0.004
		$\langle\phi_1\rangle$	0.007	0.010
	c	$\langle\phi\rangle$	0.003	0.004
		$\langle\phi_0\rangle$	0.003	0.004
		$\langle\phi_1\rangle$	0.007	0.004
1.0	a	$\langle\phi\rangle$	0.032	0.017
		$\langle\phi_0\rangle$	0.038	0.021
		$\langle\phi_1\rangle$	0.023	0.028
	b	$\langle\phi\rangle$	0.009	0.003
		$\langle\phi_0\rangle$	0.010	0.002
		$\langle\phi_1\rangle$	0.016	0.012
	c	$\langle\phi\rangle$	0.030	0.011
		$\langle\phi_0\rangle$	0.035	0.014
		$\langle\phi_1\rangle$	0.085	0.031
10.0	a	$\langle\phi\rangle$	0.367	0.234
		$\langle\phi_0\rangle$	0.381	0.242
		$\langle\phi_1\rangle$	0.276	0.187
	b	$\langle\phi\rangle$	0.080	0.013
		$\langle\phi_0\rangle$	0.082	0.013
		$\langle\phi_1\rangle$	0.053	0.044
	c	$\langle\phi\rangle$	0.182	0.122
		$\langle\phi_0\rangle$	0.178	0.121
		$\langle\phi_1\rangle$	0.329	0.202
		RMS of $E_{\langle\phi\rangle}$	0.140	0.088
		RMS of $E_{\langle\phi_0\rangle}$	0.144	0.091
		RMS of $E_{\langle\phi_1\rangle}$	0.147	0.094

Table VI. Scalar flux comparisons for case 2

			RMS Relative Error $E_{\langle\phi\rangle}$	
L	Case	Quantity	Algorithm A	Algorithm B
0.1	a	$\langle\phi\rangle$	0.010	0.010
		$\langle\phi_0\rangle$	0.011	0.011
		$\langle\phi_1\rangle$	0.003	0.003
	b	$\langle\phi\rangle$	0.004	0.004
		$\langle\phi_0\rangle$	0.004	0.004
		$\langle\phi_1\rangle$	0.007	0.007
	c	$\langle\phi\rangle$	0.004	0.004
		$\langle\phi_0\rangle$	0.004	0.004
		$\langle\phi_1\rangle$	0.003	0.004
1.0	a	$\langle\phi\rangle$	0.020	0.016
		$\langle\phi_0\rangle$	0.020	0.018
		$\langle\phi_1\rangle$	0.030	0.005
	b	$\langle\phi\rangle$	0.004	0.002
		$\langle\phi_0\rangle$	0.003	0.002
		$\langle\phi_1\rangle$	0.038	0.027
	c	$\langle\phi\rangle$	0.010	0.004
		$\langle\phi_0\rangle$	0.015	0.003
		$\langle\phi_1\rangle$	0.255	0.011
10.0	a	$\langle\phi\rangle$	0.140	0.041
		$\langle\phi_0\rangle$	0.160	0.045
		$\langle\phi_1\rangle$	0.092	0.042
	b	$\langle\phi\rangle$	0.092	0.004
		$\langle\phi_0\rangle$	0.092	0.003
		$\langle\phi_1\rangle$	0.182	0.043
	c	$\langle\phi\rangle$	0.091	0.024
		$\langle\phi_0\rangle$	0.104	0.024
		$\langle\phi_1\rangle$	0.630	0.096
		RMS of $E_{\langle\phi\rangle}$	0.064	0.017
		RMS of $E_{\langle\phi_0\rangle}$	0.071	0.019
		RMS of $E_{\langle\phi_1\rangle}$	0.237	0.039

Table VII. Scalar flux comparisons for case 3

			RMS Relative Error $E_{\langle\phi\rangle}$	
L	Case	Quantity	Algorithm A	Algorithm B
0.1	a	$\langle\phi\rangle$	0.002	0.002
		$\langle\phi_0\rangle$	0.003	0.004
		$\langle\phi_1\rangle$	0.004	0.004
	b	$\langle\phi\rangle$	0.006	0.007
		$\langle\phi_0\rangle$	0.002	0.002
		$\langle\phi_1\rangle$	0.014	0.015
	c	$\langle\phi\rangle$	0.002	0.002
		$\langle\phi_0\rangle$	0.002	0.002
		$\langle\phi_1\rangle$	0.005	0.004
1.0	a	$\langle\phi\rangle$	0.006	0.007
		$\langle\phi_0\rangle$	0.014	0.014
		$\langle\phi_1\rangle$	0.004	0.002
	b	$\langle\phi\rangle$	0.005	0.005
		$\langle\phi_0\rangle$	0.004	0.005
		$\langle\phi_1\rangle$	0.006	0.006
	c	$\langle\phi\rangle$	0.002	0.003
		$\langle\phi_0\rangle$	0.010	0.004
		$\langle\phi_1\rangle$	0.011	0.002
10.0	a	$\langle\phi\rangle$	0.149	0.059
		$\langle\phi_0\rangle$	0.284	0.143
		$\langle\phi_1\rangle$	0.061	0.022
	b	$\langle\phi\rangle$	0.028	0.004
		$\langle\phi_0\rangle$	0.029	0.004
		$\langle\phi_1\rangle$	0.030	0.019
	c	$\langle\phi\rangle$	0.089	0.067
		$\langle\phi_0\rangle$	0.151	0.077
		$\langle\phi_1\rangle$	0.410	0.113
		RMS of $E_{\langle\phi\rangle}$	0.059	0.030
		RMS of $E_{\langle\phi_0\rangle}$	0.108	0.054
		RMS of $E_{\langle\phi_1\rangle}$	0.139	0.039

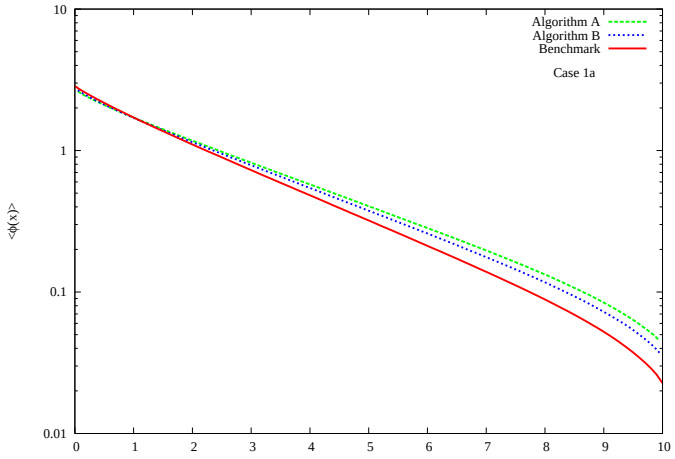

(a) $\langle \phi(x) \rangle$

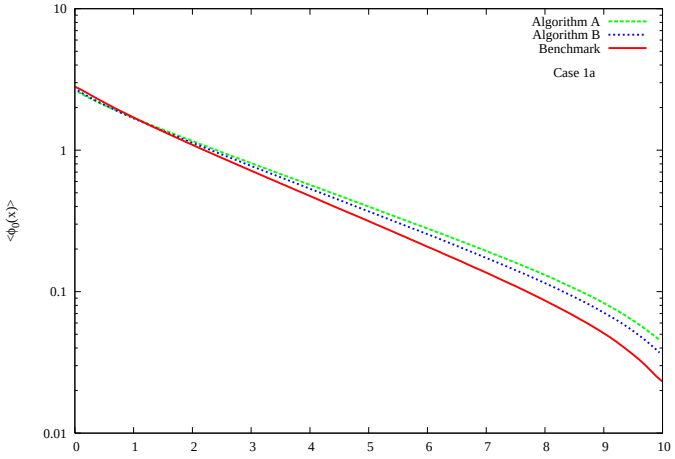

(b) $\langle \phi_0(x) \rangle$

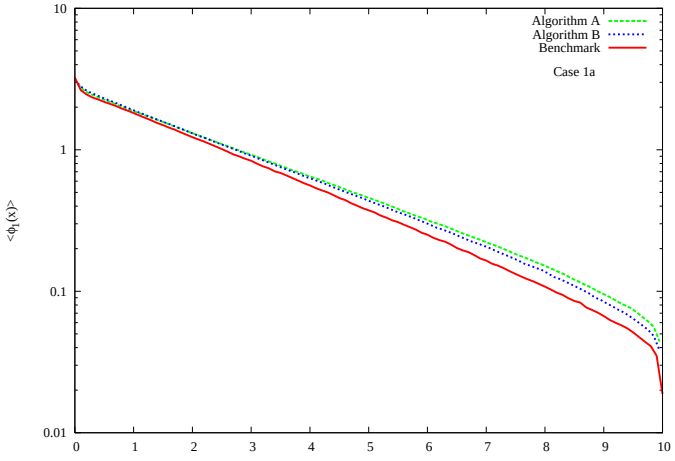

(c) $\langle \phi_1(x) \rangle$

Figure 1. Scalar flux distribution comparison for case 1a and L = 10

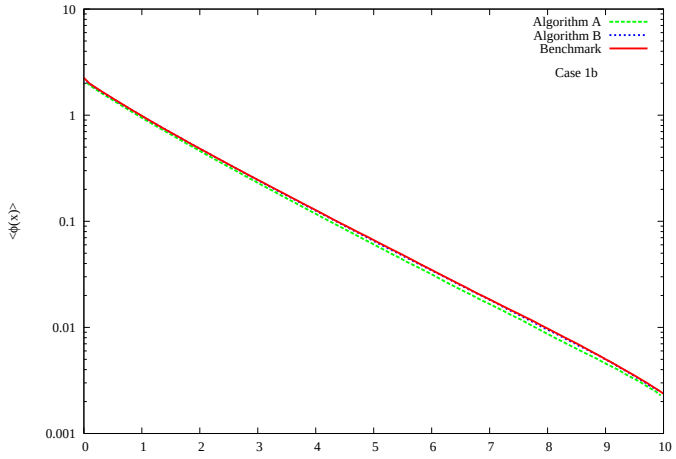

(a) $\langle \phi(x) \rangle$

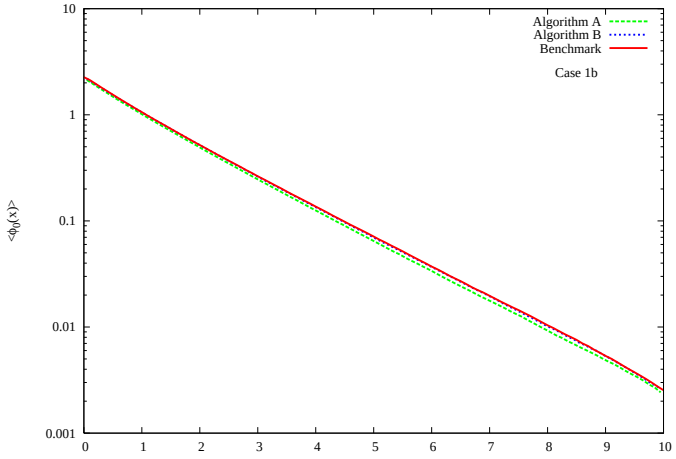

(b) $\langle \phi_0(x) \rangle$

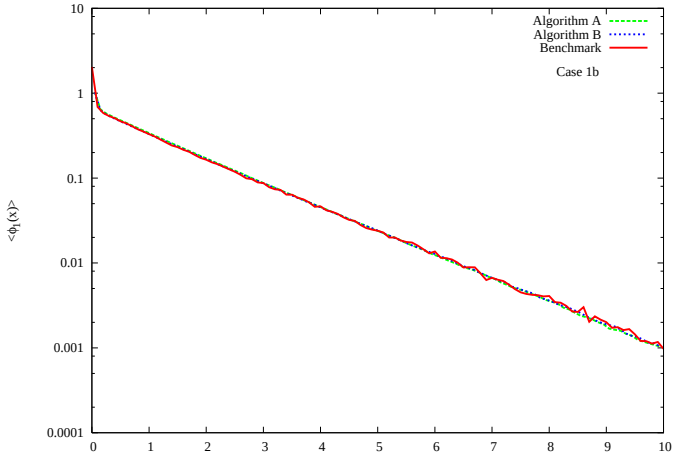

(c) $\langle \phi_1(x) \rangle$

Figure 2. Scalar flux distribution comparison for case 1b and L = 10

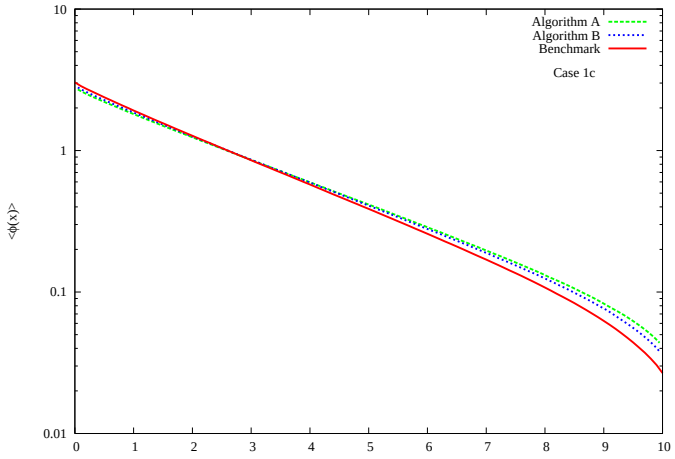

(a) $\langle \phi(x) \rangle$

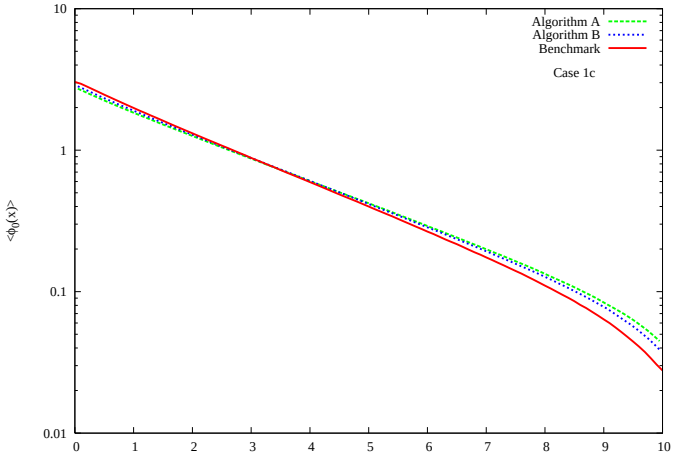

(b) $\langle \phi_0(x) \rangle$

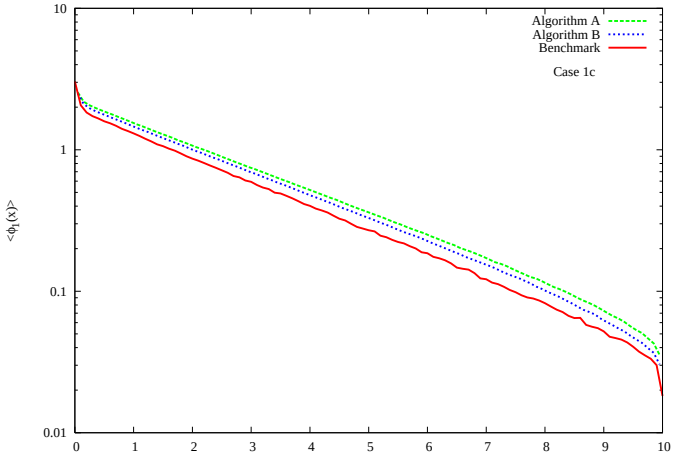

(c) $\langle \phi_1(x) \rangle$

Figure 3. Scalar flux distribution comparison for case 1c and L = 10

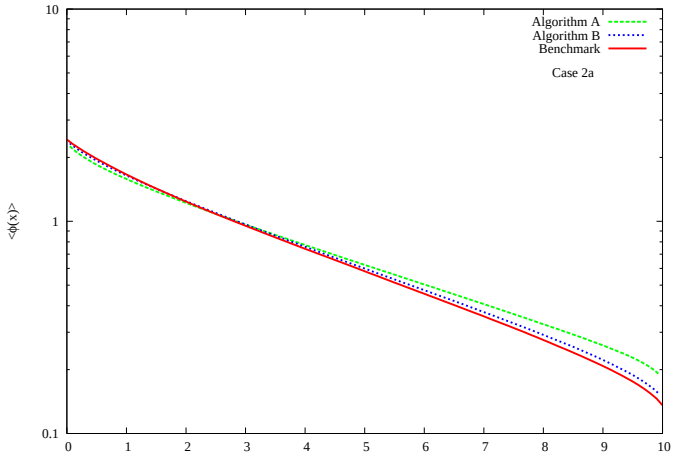

(a) $\langle \phi(x) \rangle$

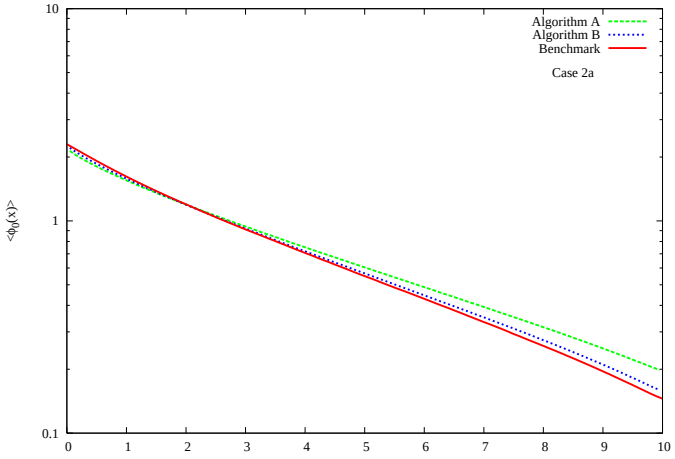

(b) $\langle \phi_0(x) \rangle$

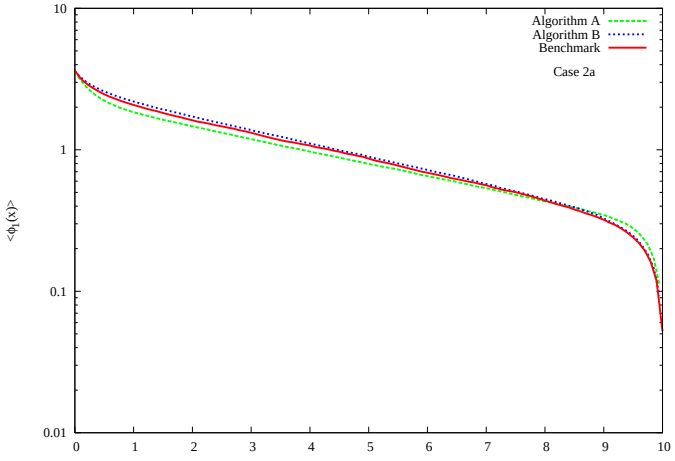

(c) $\langle \phi_1(x) \rangle$

Figure 4. Scalar flux distribution comparison for case 2a and L = 10

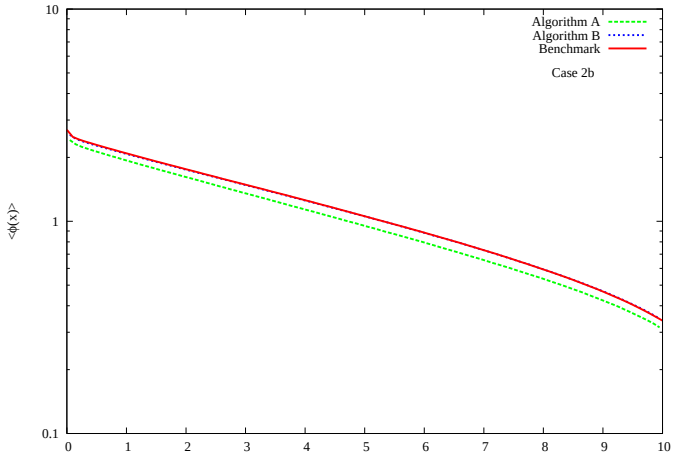

(a) $\langle \phi (x) \rangle$

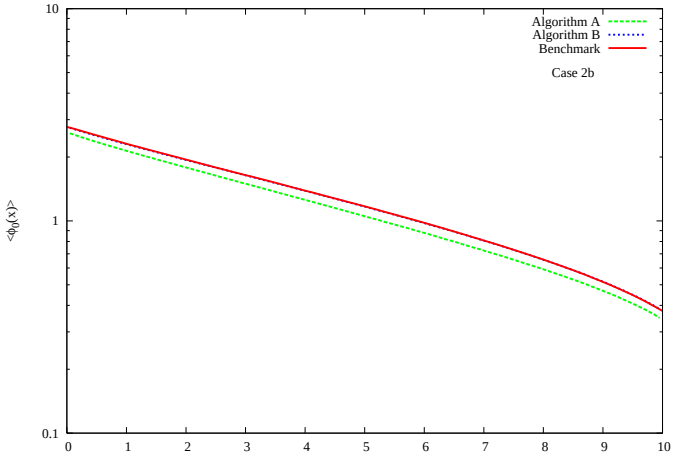

(b) $\langle \phi_0 (x) \rangle$

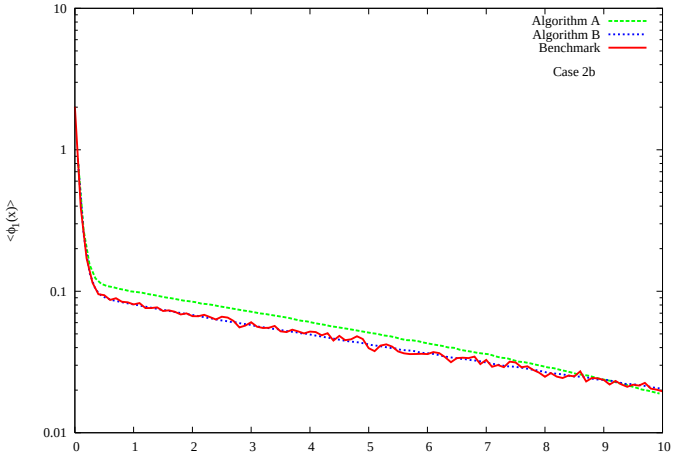

(c) $\langle \phi_1 (x) \rangle$

Figure 5. Scalar flux distribution comparison for case 2b and L = 10

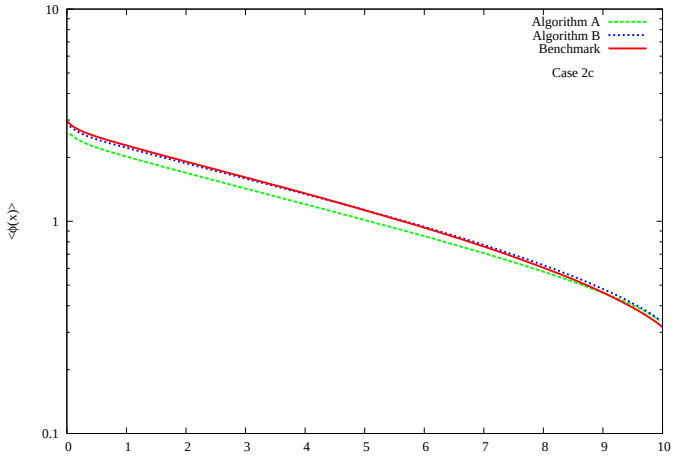

(a) $\langle \phi(x) \rangle$

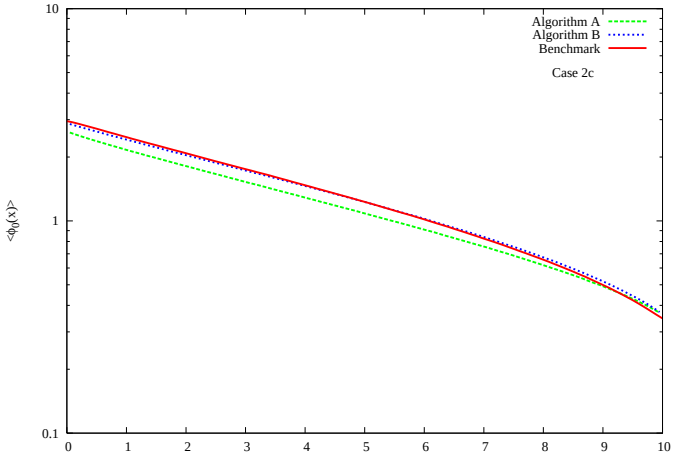

(b) $\langle \phi_0(x) \rangle$

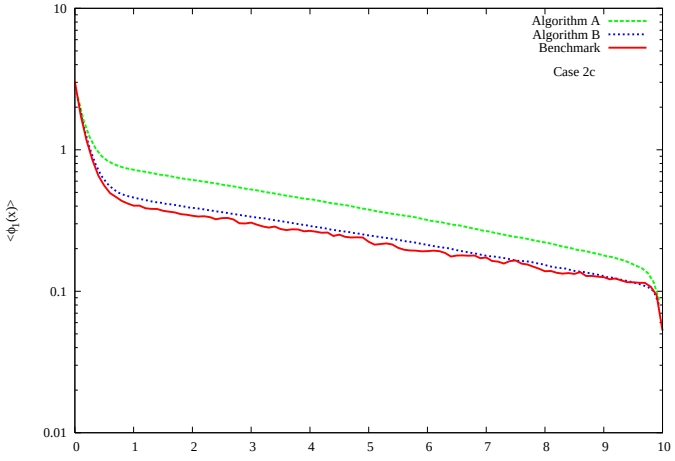

(c) $\langle \phi_1(x) \rangle$

Figure 6. Scalar flux distribution comparison for case 2c and L = 10

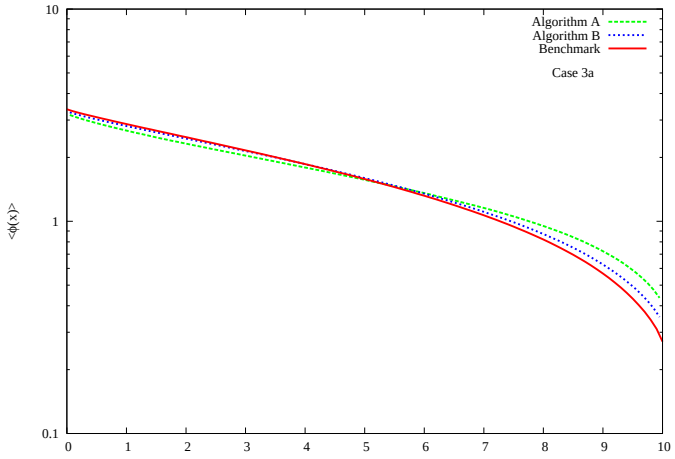

(a) $\langle \phi(x) \rangle$

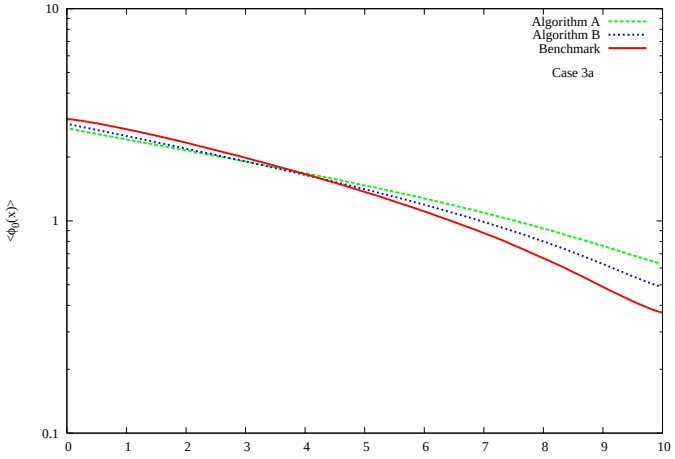

(b) $\langle \phi_0(x) \rangle$

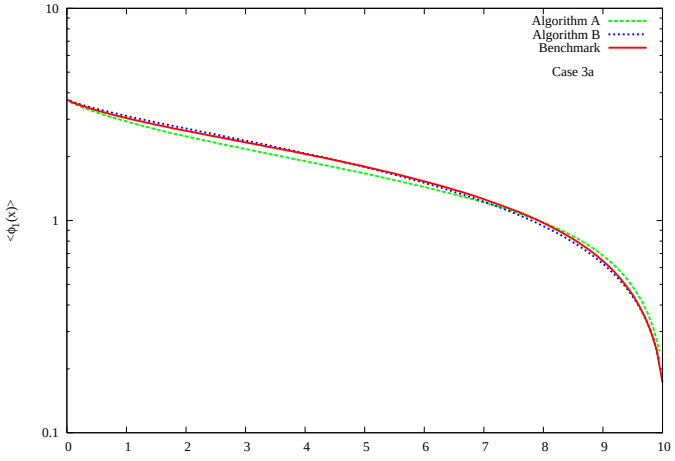

(c) $\langle \phi_1(x) \rangle$

Figure 7. Scalar flux distribution comparison for case 3a and L = 10

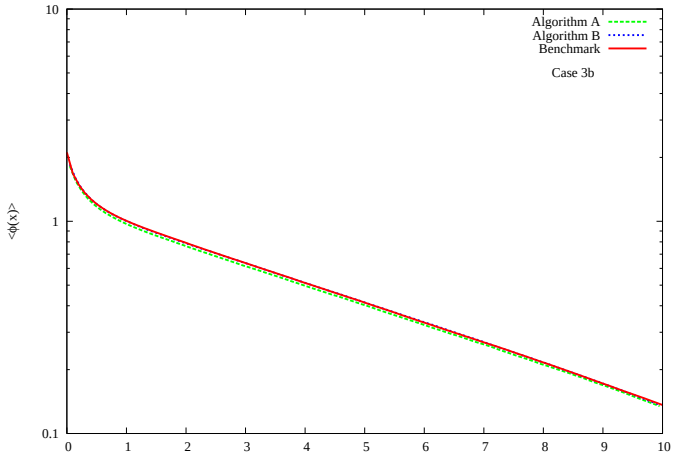

(a) $\langle \phi(x) \rangle$

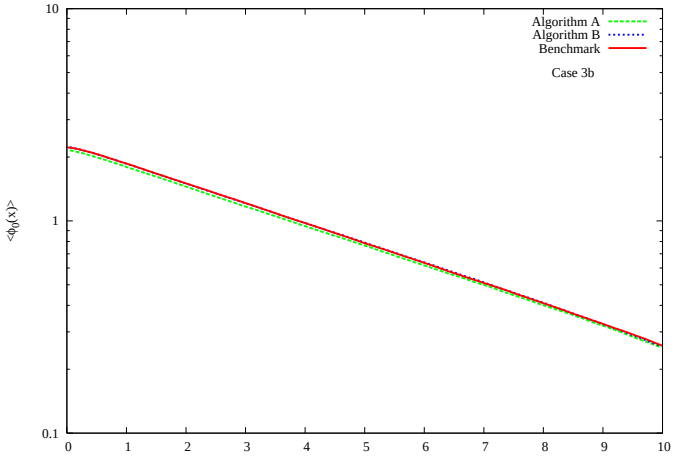

(b) $\langle \phi_0(x) \rangle$

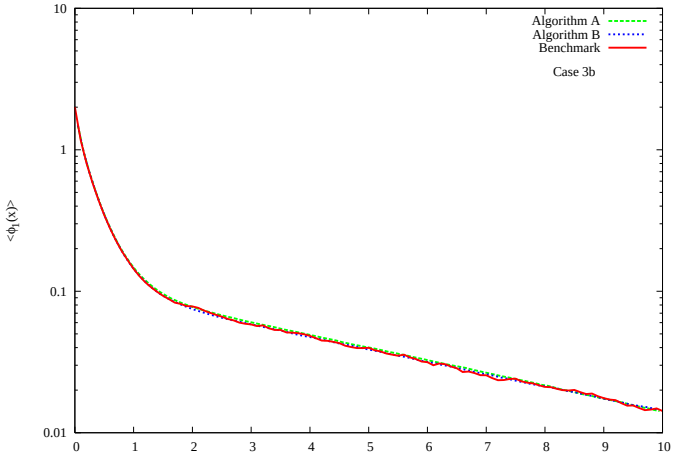

(c) $\langle \phi_1(x) \rangle$

Figure 8. Scalar flux distribution comparison for case 3b and L = 10

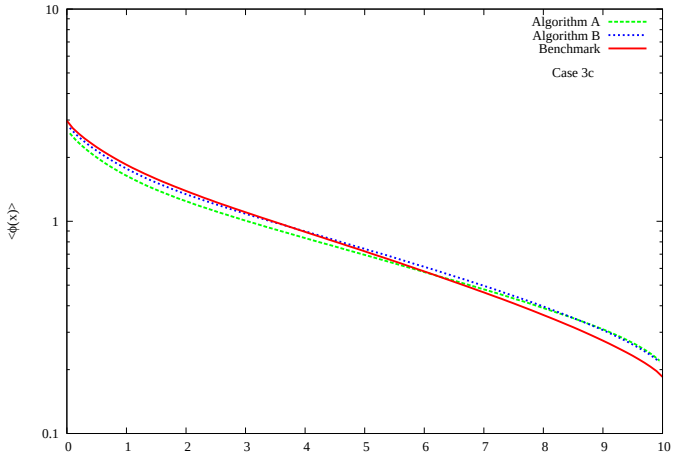

(a) $\langle \phi (x) \rangle$

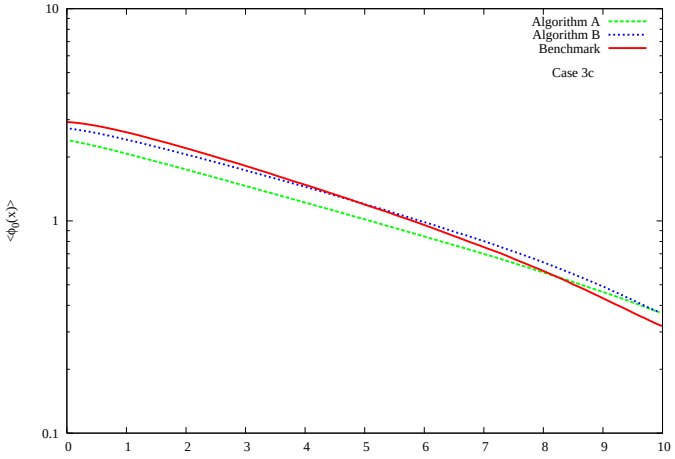

(b) $\langle \phi_0 (x) \rangle$

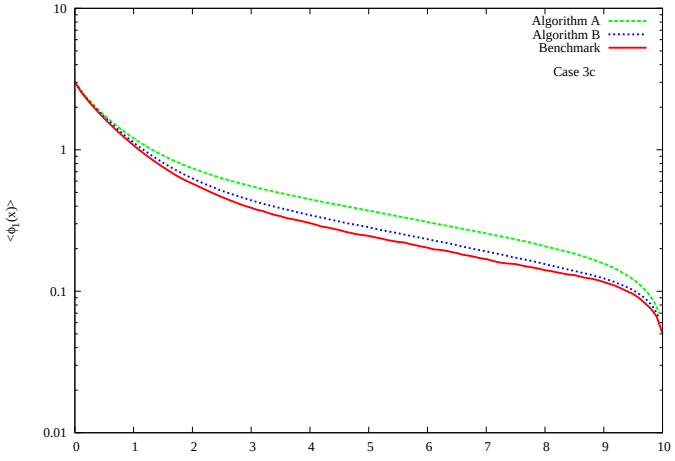

(c) $\langle \phi_1 (x) \rangle$

Figure 9. Scalar flux distribution comparison for case 3c and L = 10

ACKNOWLEDGEMENTS

This work performed under the auspices of the U.S. Department of Energy by Lawrence Livermore National Laboratory under Contract DE-AC52-07NA27344. The author is indebted to Olivier Zuchuat, who went to extraordinary measures to retrieve the available scalar flux distribution data previously published in graphical form in Ref. [7].

REFERENCES

[1] C. D. Levermore, G. C. Pomraning, D. L. Sanzo, and J. Wong, "Linear transport theory in a random medium," *J. Math. Phys.*, **27**, pp. 2526-2536 (1986).

[2] G. C. Pomraning, *Linear Kinetic Theory and Particle Transport in Stochastic Mixtures*, World Scientific Publishing Co. Pte. Ltd., River Edge, New Jersey USA (1991).

[3] G. B. Zimmerman, "Recent Developments in Monte Carlo Techniques," Lawrence Livermore National Laboratory Report UCRL-JC-105616 (1990).

[4] G. B. Zimmerman and M. L. Adams, "Algorithms for Monte-Carlo Particle Transport in Binary Statistical Mixures," *Trans. Am. Nucl. Soc.*, San Francisco, CA, November 10-14, 1991, Vol. 64, p. 287 (1991).

[5] T. J. Donovan and Y. Danon, "Application of Monte Carlo Chord-Length Sampling Algorithms to Transport Through a Two-Dimensional Binary Stochastic Mixture," *Nucl. Sci. Engr.*, **143**, pp. 226-239 (2003).

[6] M. L. Adams, E. W. Larsen, and G. C. Pomraning, "Benchmark Results for Particle Transport in a Binary Markov Statistical Medium," *J. Quant. Spectrosc. Radiat. Transfer*, **42**, pp. 253-266 (1989).

[7] O. Zuchuat, R. Sanchez, I. Zmijarevic, and F. Malvagi, "Transport in Renewal Statistical Media: Benchmarking and Comparison With Models," *J. Quant. Spectrosc. Radiat. Transfer*, **51**, pp. 689-722 (1994).

[8] E. E. Lewis and W. F. Miller, *Computational Methods of Neutron Transport*, American Nuclear Society, Lagrange Park, Illinois, USA (1993).

[9] O. Zuchuat, personal communication (2008).